

# Nanoscale

Accepted Manuscript



This is an *Accepted Manuscript*, which has been through the Royal Society of Chemistry peer review process and has been accepted for publication.

*Accepted Manuscripts* are published online shortly after acceptance, before technical editing, formatting and proof reading. Using this free service, authors can make their results available to the community, in citable form, before we publish the edited article. We will replace this *Accepted Manuscript* with the edited and formatted *Advance Article* as soon as it is available.

You can find more information about *Accepted Manuscripts* in the [Information for Authors](#).

Please note that technical editing may introduce minor changes to the text and/or graphics, which may alter content. The journal's standard [Terms & Conditions](#) and the [Ethical guidelines](#) still apply. In no event shall the Royal Society of Chemistry be held responsible for any errors or omissions in this *Accepted Manuscript* or any consequences arising from the use of any information it contains.

## ARTICLE

## Titania nanobundle networks as dye-sensitized solar cells photoanodes

Cite this: DOI: 10.1039/x0xx00000x

Cunku Dong<sup>a,b</sup>, Wanchun Xiang<sup>a</sup>, Fuzhi Huang<sup>c</sup>, Dongchuan Fu<sup>c</sup>, Wenchao Huang<sup>c</sup>, Udo Bach<sup>c,d,e</sup>, Yi-Bing Cheng<sup>c</sup>, Xin Li<sup>b,\*</sup> and Leone Spiccia<sup>a,\*</sup>

Received 00th January 2012,  
Accepted 00th January 2012

DOI: 10.1039/x0xx00000x

www.rsc.org/

Quasi-one-dimensional (1D) titania nanobundles were synthesized via a hydrothermal method and used to print random network nanostructured films. These films are shown to be ideally suited for application as photoanodes in dye-sensitized solar cells (DSCs) as they have a higher porosity compared to the traditional 1D nanostructured TiO<sub>2</sub> materials. Devices constructed using the N719 dye and iodide/triiodide as redox mediator in the electrolyte yielded energy conversion efficiencies ( $\eta = 6.1 \pm 0.2\%$ ), which were marginally lower than for devices made with the commonly used P25 titania films ( $\eta = 6.3 \pm 0.1\%$ ) at one sun simulated solar radiation. Application of an electrolyte based on the [Co(bpy)<sub>3</sub>]<sup>2+/3+</sup> redox couple and the MK2 organic sensitizer, resulted in higher efficiencies ( $\eta = 7.70 \pm 0.1\%$ ) than for the P25 devices ( $\eta = 6.3 \pm 0.3\%$ ). Each performance parameter (short circuit current density, open circuit voltage and fill factor) was higher for the TiO<sub>2</sub> nanobundle devices than those for the P25-based devices. The results of electrochemical impedance spectroscopy (EIS), intensity-modulated photovoltage spectroscopy (IMVS), and dye-loading measurements indicated that the better performance of TiO<sub>2</sub> nanobundle devices with cobalt electrolyte correlates with higher porosity, relatively fast electron transport and more efficient suppression of electron recombination. A faster rate of diffusion of the cobalt complexes through the highly porous TiO<sub>2</sub> nanobundle network is proposed to contribute to the enhanced device efficiency.

### Introduction

In recent decades, tremendous efforts have been devoted to the development of new photovoltaic devices or the enhancement of the energy conversion efficiency of existing solar cells in order to ease energy and environmental pressures arising from the excessive consumption of fossil fuels. Amongst the various photovoltaic technologies, dye-sensitized solar cells (DSCs) are highly promising next-generation devices,<sup>1</sup> which have the potential advantages of low-cost fabrication, ease of processing and relatively high power conversion efficiency (PCE).<sup>2</sup> The current record conversion efficiency of 12.3% was achieved using cobalt redox couple based DSCs in combination with an organic dye (Y123) and a porphyrin dye (YD2-o-C8). This new milestone stimulates the further development of non-iodide based electrolytes for DSCs.<sup>3</sup> Our group has introduced several new redox mediators DSCs, such as ferrocene and its derivatives,<sup>4-6</sup> cobalt pentapyridyl and hexapyridyl complexes.<sup>7,8</sup> In addition, the [Fe(CN)<sub>6</sub>]<sup>4-/3-</sup> and [Co(bpy)<sub>3</sub>]<sup>2+/3+</sup> (bpy = 2,2'-bipyridine) complexes were employed in aqueous DSC electrolytes.<sup>9,10</sup>

One factor that limits the energy conversion efficiency is electron recombination at the semiconductor interface in which the injected electrons either react with oxidized redox species in the electrolyte or with the oxidized dye during the operation of the DSCs.<sup>11</sup> To date, various one-dimensional (1D) nanomaterials (e.g., nanotubes, nanorods and nanowires) have been applied as photoanodes in DSCs in an effort to reduce energy losses through recombination.<sup>12-19</sup> In particular, nanowires (and nanorods) have been demonstrated to possess better electron mobility than the conventional semiconductor nanoparticle networks and to inhibit electron recombination because of a significant reduction in the number of boundary contacts between the nanoparticles.<sup>20</sup> Despite the unique electron transport properties, the limited internal surface area (11 m<sup>2</sup>/g)<sup>21</sup> of such 1D TiO<sub>2</sub> nanomaterials is a major drawback as it results in insufficient dye loading and, thereby, poor light absorption in comparison with commonly used nanoparticles.<sup>22,23</sup> Consequently, the PCE of DSCs based on pure TiO<sub>2</sub> nanowires is around 5%, which is lower than that achieved by devices fabricated with TiO<sub>2</sub> nanoparticles.<sup>24</sup> Efforts have been made to improve the PCE of TiO<sub>2</sub> nanowire-based DSCs by using much longer nanowires (up to 8  $\mu\text{m}$ ).<sup>25</sup> Lower photocurrent densities were, however, observed which

were proposed to result from the widening and fusion of the nanowires at the base of the films. This led to a decrease in nanowire packing density and lower transmittance of the incident light with increasing nanowire length.<sup>25</sup> In order to address these problems, 1D TiO<sub>2</sub> (or ZnO)-based nanostructured materials have been developed with the aim of increasing the internal surface area.<sup>26-30</sup> The incorporation of 1D nanostructures into nanoparticles has proven an effective route for improving light harvesting,<sup>31-33</sup> by increasing the surface area<sup>34-36</sup> whilst maintaining good charge transport through the film.<sup>37-40</sup> For example, Wang et al. showed that 1D ZnO nanowires grown in situ within mesoporous TiO<sub>2</sub> nanoparticle films effectively scatter incident light and offer a unidirectional pathway for electron transport in the hybrid films.<sup>41</sup> Kuang et al. reported a novel TiO<sub>2</sub> nanowire/nanoparticles hierarchical photoanode with superior light scattering and lower rates of electron recombination.<sup>42</sup> These promising studies highlight the value of applying well-preformed nanomaterials for the construction of hierarchical nanostructured photoanodes. Hence, it is becoming clear that there are benefits in developing novel nanostructured materials for use as hierarchical photoanodes in DSCs, which combine the advantages of 1D nanomaterials and conventional nanoparticles - efficient suppression of recombination observed for 1D nanomaterials with the large surface area of 0D nanomaterials.

Herein, we report the application of a novel TiO<sub>2</sub> nanonetwork (TiO<sub>2</sub>NN) morphology, consisting of quasi-1D nanobundles with a large surface area, in DSCs. The TiO<sub>2</sub> nanobundles were synthesized from titanium(IV) butoxide by a hydrothermal method<sup>43</sup> and used to develop a paste for depositing photoanode films for DSC construction. The resulting TiO<sub>2</sub> nanobundle nanonetwork shows a good dye-loading capacity and mass transport of the redox mediator compared to common nanoparticle based titania films. DSCs constructed with these thin photoanode films and the [Co(bpy)<sub>3</sub>]<sup>2+/3+</sup> electrolyte (bpy = 2,2'-bipyridine) reach PCEs of 7.7%, higher than that for analogous DSCs prepared using P25 films (6.3%), a widely studied material frequently used for the purpose of performance comparison.

## Experimental section

### Materials

Unless otherwise specified, all reagents, solvents and chemicals were obtained from either Sigma-Aldrich or Merck Specialty Chemicals and were used as received. The P25 TiO<sub>2</sub> powder (70% anatase and 30% rutile, particle size 21 nm) was purchased from Evonik Degussa. The N719 dye, bis (tetrabutyl ammonium) cis-bis(isothiocyanato)-bis(2,2'-bipyridyl-4,4'-di carboxylato) ruthenium(II), was purchased from Dyesol and purified using column chromatography on Sephadex LH20 using methanol as eluent, following published methodology.<sup>44</sup> MK2 was purchased from Sigma-Aldrich. [Co(bpy)<sub>3</sub>](TFSI)<sub>2</sub> and [Co(bpy)<sub>3</sub>](TFSI)<sub>3</sub> were prepared by a published method.<sup>45</sup>

### Hydrothermal synthesis of TiO<sub>2</sub> nanobundles

The TiO<sub>2</sub> nanobundles were synthesized according to previous literature.<sup>43</sup> Briefly, 485 mg of lithium chloride was first dissolved in a mixture of N,N-dimethylformamide (30 mL) and acetic acid (20 mL). Titanium(IV) butoxide (10 mL, 97%) was added and the obtained solution was transferred into a Teflon-lined stainless steel autoclave (100 mL) and heated in an oven at 200 °C for 20 h. The as-synthesized TiO<sub>2</sub> nanobundles were thoroughly washed four times with 200 mL absolute ethanol and collected following centrifugation. They were stored without desiccation or drying until used in paste preparation to avoid aggregation induced by the drying process.

### Preparation of TiO<sub>2</sub> pastes and working electrodes

The as-prepared TiO<sub>2</sub> nanobundles (2.00 g) were suspended in 100 mL of absolute ethanol, stirred at room temperature for 2 h and then sonicated for 1 h. Ethyl cellulose (EC, 1.00 g) powder was dissolved in 100 mL of absolute ethanol and mixed with the TiO<sub>2</sub> nanobundles suspension. Following sonication for 1 h, the mixture was stirred overnight and then terpineol (8.69 mL) was added dropwisely into the mixture. Subsequently, the ethanol in TiO<sub>2</sub> nanobundles/ethyl cellulose/terpineol suspension was removed using a rotary evaporator at 40°C and 150 mPa. A similar procedure was followed to prepare the P25 paste. In this case, we used 2.0 g P25 powder, 1.6 g EC and 8.69 mL terpineol for the MK2 + [Co(bpy)<sub>3</sub>]<sup>2+/3+</sup> based DSCs and 2.0 g P25 powder, 1.6 g EC and 8.69 mL terpineol for the N719 + I<sup>-</sup>/I<sub>3</sub><sup>-</sup> based DSCs.

### DSC fabrication

The 3.0 μm and 6.0 μm TiO<sub>2</sub> nanobundle (and P25 nanoparticles) films were screen-printed on fluorine-doped SnO<sub>2</sub> (FTO) conducting glass substrates (10 Ω/□). A 4.0 μm scattering layer composed of 400 nm-sized TiO<sub>2</sub> particles was then screen-printed on top of the TiO<sub>2</sub> nanobundle (and P25 nanoparticles) films. The screen-printed photoanodes were sintered at 450 °C for 30 min and 500 °C for 15 min. The sintered titania photoanodes were treated with 40 mM TiCl<sub>4</sub> aqueous solution, and then sintered at 500 °C for 30 min. After cooling down to 80 °C, these photoanode films were immersed into a dye solution, either 0.5 mM N719 dye in acetonitrile/tert-butanol mixed solution (1:1, v/v) for 24 h or 0.3 mM MK2 dye in acetonitrile/toluene/tert-butanol mixture (1:1:1, v/v/v) for 12 h at room temperature. The sensitized photoanode films were rinsed with acetonitrile or toluene, respectively, to remove any physisorbed dye.

The platinized counter electrodes were prepared by thermal decomposition of H<sub>2</sub>PtCl<sub>6</sub> solution (10 mM in isopropanol) onto FTO glass at 400 °C for 15 min. The working electrodes and counter electrodes were sealed together by hot melting of a 25 μm Surlyn gasket (Solaronix). The electrolyte was vacuum filled into the space between working electrode and counter electrodes through holes drilled on the back of the counter electrode. The iodide/triiodide electrolyte used in this study was composed of 0.60 M 1-methyl-3-propylimidazolium iodide

(PMII), 0.10 M guanidinium thiocyanate, 0.03 M  $I_2$ , 0.50 M tert-butylpyridine (*t*BP) dissolved in an acetonitrile/valeronitrile mixture (85:15, v/v). The  $[Co(bpy)_3]^{2+/3+}$  electrolyte consisted of 0.20 M  $[Co(bpy)_3](TFSI)_2$ , 0.060 M  $[Co(bpy)_3](TFSI)_3$ , 0.050 M LiTFSI and 1.00 M tert-butylpyridine in acetonitrile.

### Characterization

The dye loading amount on films was measured by desorbing the dye from the photoanodes using a 0.10 M KOH in water for N719 and a 0.10 M KOH in acetonitrile/toluene/tert-butanol mixture (1:1:1, v/v/v) containing a small amount of methanol for MK2. The UV-Visible spectrum of the solution containing desorbed dye was recorded using a Perkin-Elmer Lambda 950 spectrophotometer. The dye loading amounts were determined by reading the measured absorbance value of each dye from the calibration curves plotting the absorbance versus concentration of a series of dye solution (the plots were linear indicating adherence to the Lambert-Beer law).

Current-voltage (*J*-*I*) curves of the solar cells were obtained using a Keithley 2400 source meter under illumination of simulated sunlight (100 mW/cm<sup>2</sup>) offered by an Oriel solar simulator. The intensity was calibrated with a silicon reference diode (Fraunhofer). The incident-photon-to-current efficiency (IPCE) spectra were measured over the 350 - 800 nm wavelength range using a Keithley 2400 source meter.

Electrochemical impedance spectroscopy (EIS) measurements were conducted on a potentiostat (BioLogic VSP) with a frequency range of 0.5-10<sup>5</sup> Hz at open-circuit voltage in dark. The measured cells were fabricated with the standard procedure described above using TiO<sub>2</sub>NN or P25 photoanode together with the corresponding electrolyte (cobalt or iodide).

Intensity-modulated photovoltage/photocurrent spectroscopy (IMVS/IMPS) measurements were performed on an ECW IM6 electrochemical workstation with a frequency response analyzer and a support unit (potentiostat/galvanostat), a 'slave' potentiostat controlling the amplitude and modulation of the light source over a wide range of frequencies (0.01-10<sup>5</sup> Hz). The amplitude of the sinusoidal modulation for these measurements was less than 5% under the illumination provided by a 435 nm light emitting diode. The Ziew software was used to obtain the electron transport and recombination time by fitting the resultant plots.

Surface areas and pore sizes were determined via the Brunauer-Emmett-Teller (BET) method using QuadraSorb Station 2 instrument. The samples were outgassed at 300 °C for 30 h prior to the experiment.

## Results and discussion

### Preparation, Morphology and Structure of the TiO<sub>2</sub> Nanobundle Network Films

The TiO<sub>2</sub> nanobundles were synthesized via a hydrothermal method from a mixture of N,N-dimethylformamide (DMF) and acetic acid (HAc) containing lithium chloride (LiCl) as an

additive.<sup>43</sup> The morphology and structure of the TiO<sub>2</sub> nanobundle network (TiO<sub>2</sub>NN) was first characterized by X-ray diffraction (XRD) analysis and field-emission scanning electron microscopy (FE-SEM). Fig. 1a shows the XRD patterns of the as-prepared primitive and annealed TiO<sub>2</sub>NN. The diffraction peaks of the as prepared and annealed samples correspond well to those of the TiO<sub>2</sub> anatase phase with the obvious co-existence of some rutile (blue circle) and brookite impurities (yellow asterisk). The TiO<sub>2</sub>NN nanocrystalline structure is not affected by annealing, in agreement with a previous study by Lou *et al.*<sup>43</sup> However, the diffraction peaks of the anatase TiO<sub>2</sub> nanobundles increase in intensity on annealing, indicating an increase in crystallinity.

Field Emission Scanning Electron Microscopy (FE-SEM) was performed to characterize the morphology of the as-prepared TiO<sub>2</sub>NN. As shown in Fig. 1b, the primitive TiO<sub>2</sub>NN materials have a uniform size distribution and a hierarchical nanostructure, which consists of a central flower-like framework from which bundles of nanowires extend. These bundles are typically several hundred nanometers in length and ~20 nm in diameter, much like the long antennae protruding from the body of a sea anemone. They significantly increase the surface area and could therefore enhance the dye loading capability compared to the well-ordered rutile TiO<sub>2</sub> nanowire arrays.<sup>19</sup> This morphology favours the unidirectional electron transport in a single nanobundle.

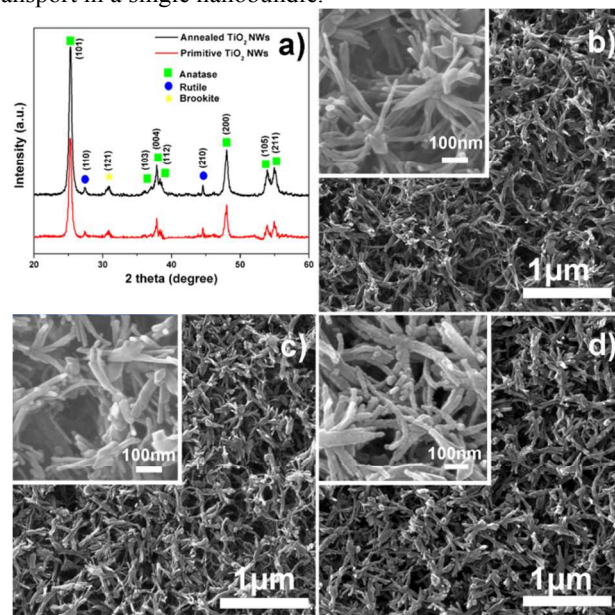


**Fig. 1** a) XRD patterns of the as prepared and annealed TiO<sub>2</sub>NN films. SEM images of: b) as prepared TiO<sub>2</sub>NN film; c) annealed TiO<sub>2</sub>NN film; d) TiCl<sub>4</sub>-treated TiO<sub>2</sub>NN film after annealing. For each sample, the high-resolution image is inserted in the low-resolution SEM.

A paste was developed from the TiO<sub>2</sub>NN material which was used to screen-print photoanode films for DSC construction. Printing and sintering of the TiO<sub>2</sub>NN films on the FTO glass did not change the morphology, as clearly shown by the SEM image of a typical sintered film in Fig. 1c. The printed films consist of random, interleaved TiO<sub>2</sub> nanonetworks. The large

pores formed by the interleaving of the TiO<sub>2</sub> nanobundles in the large-scale random nanonetwork could be particularly advantageous for the diffusion of the relatively large [Co(bpy)<sub>3</sub>]<sup>2+/3+</sup> complexes (see transient photocurrent measurements below). Additionally, better transport of the cobalt redox couples within the TiO<sub>2</sub>NN film would be possible as a result of the larger pores of the TiO<sub>2</sub>NN films (average pore volume, 0.86 cm<sup>3</sup>/g), compared with the P25 films (average pore volume, 0.66 cm<sup>3</sup>/g). The BET results, on the other hand, indicated that the specific surface area of the TiO<sub>2</sub>NN, films, 38 m<sup>2</sup>/g, is similar to that of the P25 films (36–41 m<sup>2</sup>/g, depending on film thickness). Interestingly, after TiCl<sub>4</sub>-treatment the surface roughness of the TiO<sub>2</sub> nanobundles increases and tiny TiO<sub>2</sub> nanoparticles appear on their surface (Fig. 1d), resulting in more connectivity point between nanobundles.

### Solar cell performance

The *J-V* curves of DSCs constructed with the same thickness TiO<sub>2</sub>NN and P25 photoanodes in combination with N719 and MK2 and either iodide or cobalt electrolytes are shown in Fig. 2. Table 1 summarizes the average photovoltaic performance data, including short-circuit current density (*J*<sub>sc</sub>), open-circuit voltage (*V*<sub>oc</sub>), fill factor (*FF*) and PCE (*η*), obtained from four optimized cells constructed with 3 μm (MK2) and 6 μm (N719) TiO<sub>2</sub>NN films and, for comparison, P25. The photovoltaic data for experiments optimizing the thickness of TiO<sub>2</sub>NN films for use in combination with either the cobalt or the iodide electrolytes are presented in Table S1. In the case of the I<sup>-</sup>/I<sub>3</sub><sup>-</sup> redox couple, the TiO<sub>2</sub>NN-based solar cells exhibit comparable energy conversion efficiencies to devices made with the P25 nanoparticles, but better than has been reported in the literature for devices based on conventional 1D rutile TiO<sub>2</sub> nanowires (*η* = 5.1%).<sup>24</sup> The TiO<sub>2</sub>NN devices based on MK2 and cobalt electrolytes display higher *J*<sub>sc</sub>, *FF*, *V*<sub>oc</sub> and PCE than equivalent devices made with the P25 nanoparticles (see Table 1), resulting in a 23% increase in efficiency.

As will be discussed further below, the higher *J*<sub>sc</sub>, *FF* and PCE for the cobalt electrolyte based DSCs is proposed to originate from a reduction in electron recombination and efficient transport of redox active species through the electrolyte. Considering the lower molar extinction coefficient of N719 (~14,000 M<sup>-1</sup> cm<sup>-1</sup>), when compared to MK2 (~38,000 M<sup>-1</sup> cm<sup>-1</sup>),<sup>46</sup> thicker 6 μm TiO<sub>2</sub>NN films were used to achieve relatively high *J*<sub>sc</sub> and PCE (see Table 1). Since the photocurrent density depends on the amount of dye loaded on

the TiO<sub>2</sub> films, quantification was carried out by dye loading measurement followed by UV-Visible analysis, as described in the Experimental Section. The amount of MK2 adsorbed on the TiO<sub>2</sub>NN photoanode was slightly lower than on the P25 photoanode (see Table 1). Hence, despite the slightly lower dye loading, the devices based on the TiO<sub>2</sub>NN films convert incident photons into electrons more efficiently (possibly due to electron recombination), and generate a higher photocurrent density. Similar dye loadings were expected from the minor differences in the specific surface areas of the TiO<sub>2</sub>NN and P25 films determined from BET analysis (vide supra).

Additionally, the performance of DSCs can be influenced by other (photo)electronic processes occurring within the DSCs. The dark current is considered to be a good reflection of the extent of electron recombination during DSC operation, although the condition across the photoanode film differ from those under sunlight illumination.<sup>47</sup> The TiO<sub>2</sub>NN-based cells have a lower dark current density, at the same potential, for both the cobalt and iodide electrolytes (Fig. 2). This result could be taken to indicate that the recombination of electrons injected into the conduction band of TiO<sub>2</sub> with reduced redox species is suppressed in the TiO<sub>2</sub>NN devices, which was subsequently confirmed by EIS and IMVS analysis. The suppression of recombination is attributed to the unique nanonetwork morphology of TiO<sub>2</sub>NN film.

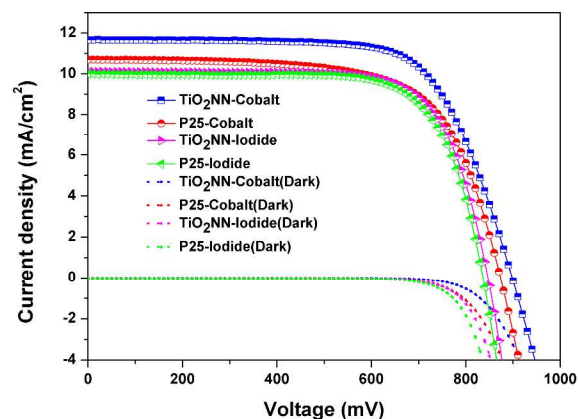


**Fig. 2** Photocurrent density (*J*) versus voltage (*V*) characteristics of DSCs constructed with N719 + I<sup>-</sup>/I<sub>3</sub><sup>-</sup> and MK2 + [Co(bpy)<sub>3</sub>]<sup>2+/3+</sup>. The dotted lines represent the corresponding *J-V* curves measured in the dark. For the electrolyte compositions see footnotes to Table 1.

## ARTICLE

**Table 1** Photovoltaic properties of DSCs with different dyes (N719 and MK2) and their corresponding redox mediators ( $I^-/I_3^-$  and  $[Co(bpy)_3]^{2+/3+}$ ).

Sample	Dye and redox couple	Film thickness [ $\mu\text{m}$ ]	$V_{oc}$ [mV]	$J_{sc}$ [ $\text{mA}/\text{cm}^2$ ]	FF	$\eta$ [%]	Adsorbed dye [ $\text{nmol cm}^{-2}$ ]
TiO <sub>2</sub> NN	MK2 + $[Co(bpy)_3]^{2+/3+}$ <sup>a</sup>	3.0±0.1	895±5	11.73±0.06	0.74±0.03	7.70±0.10	77.6±3.0
	N719 + $I^-/I_3^-$ <sup>b</sup>	6.0±0.2	847±4	10.00±0.13	0.72±0.01	6.08±0.16	75.3±3.0
P25	MK2 + $[Co(bpy)_3]^{2+/3+}$ <sup>a</sup>	3.0±0.1	873±4	10.70±0.18	0.67±0.03	6.27±0.30	84.9±0.1
	N719 + $I^-/I_3^-$ <sup>b</sup>	6.0±0.2	851±5	10.67±0.06	0.69±0.01	6.30±0.14	79.0±3.5

<sup>a</sup> Cobalt electrolyte contained 0.20 M  $[Co(bpy)_3](TFSI)_2$ , 0.060 M  $[Co(bpy)_3](TFSI)_3$ , 0.050 M LiTFSI and 1.00 M tertiary-butylpyridine (*t*BP) in acetonitrile.

<sup>b</sup> Iodide electrolyte contained 0.60 M 1-methyl-3-propylimidazolium iodide (PMII), 0.10 M guanidinium thiocyanate, 0.03 M  $I_2$ , 0.50 M *t*BP dissolved in an acetonitrile/valeronitrile mixture (85:15, v/v). The photoanode consisted of either a 3  $\mu\text{m}$  or a 6  $\mu\text{m}$  transparent layer (TiO<sub>2</sub>NN or P25) and a 4  $\mu\text{m}$  TiO<sub>2</sub> scattering layer (400 nm).

Incident photon-to-current conversion efficiency (IPCE) measurements (Fig. 3) were performed to further analyze the origin of the better photovoltaic performance of DSCs using the TiO<sub>2</sub>NN films. For the cobalt electrolyte, the maximum IPCE values for TiO<sub>2</sub>NN and P25-based devices were 76% and 70%, respectively. Notably, the cells made with TiO<sub>2</sub>NN show obviously higher IPCE values than those made with P25 over quite a wide range of wavelengths (400–700 nm). This then contributes to a higher short-circuit current density and an increase in PCE (Table 1). The higher IPCE mainly is proposed to result from efficient transport of redox couples in TiO<sub>2</sub>NN films. In contrast, for the N719-based devices mass transport of iodide electrolyte has relatively little effect on the IPCE curves above 575 nm, but in this case the situation is complicated due to competing light absorption by the iodide/triiodide electrolyte.

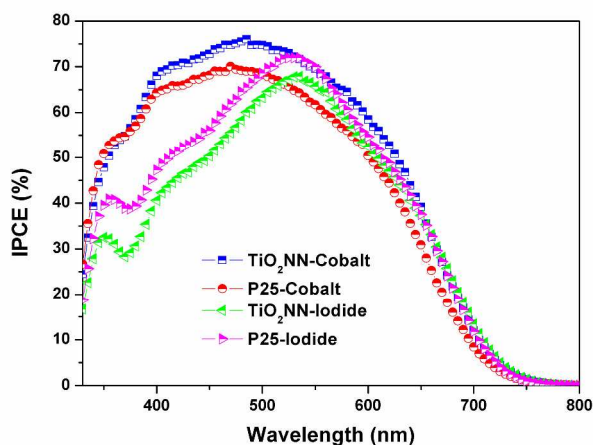


**Fig. 3** IPCE spectra of DSCs based on TiO<sub>2</sub>NN and P25 and either the cobalt or iodide-based electrolytes (see footnotes to Table 1).

Considering the larger molecular volume of  $[Co(bpy)_3]^{2+/3+}$  (6900  $\text{\AA}^3$ ) compared to iodide/triiodide (160  $\text{\AA}^3$  for  $I_3^-$ ),<sup>48</sup> mass transport through the electrolyte could influence the performance of the solar cells. Therefore, photocurrent transient measurements were carried out to evaluate the photoelectrochemical properties of TiO<sub>2</sub>NN through modulation (on/off) of the incident light.<sup>49</sup> The transient photocurrent produced under simulated AM 1.5 G one sun (Fig. 4), is slightly higher for the TiO<sub>2</sub>NN-based cells (10.5  $\text{mA}/\text{cm}^2$ ) compared with P25 (10.0  $\text{mA}/\text{cm}^2$ ). The photocurrent drops to a constant value within for the TiO<sub>2</sub>NN-based cells (0.45 s) at a slightly faster rate than for the P25 based devices (0.75s). The difference between the initial and steady-state photocurrent is also smaller for the TiO<sub>2</sub>NN devices (0.3  $\text{mA}/\text{cm}^2$ ) than for the P25 devices (0.5  $\text{mA}/\text{cm}^2$ ), indicating slightly faster mass transport of the cobalt complexes through the porous interlaced nanobundle network (see SEM).

Electrochemical impedance spectroscopy (EIS) was conducted to investigate the electron recombination of the injected electrons with the electrolyte. In DSCs, three semicircles are typically observed in Nyquist plots derived from EIS, viz., low-frequency ( $R_{diff}$ , 0.1–10 Hz), intermediate-frequency ( $R_{rs}$ , 10–10<sup>2</sup> Hz) and high-frequency ( $R_{ct}$ , 10<sup>2</sup>–10<sup>5</sup> Hz) regions, which are assigned to Warburg diffusion of redox active species in the electrolyte, electron transfer at TiO<sub>2</sub> photoanode/electrolyte hetero-interface and the redox reaction at the electrolyte/Pt counter electrode, respectively.<sup>50–52</sup> Fig. 5 shows the Bode and Nyquist plots measured under dark condition for DSCs based on TiO<sub>2</sub>NN and P25 with the two dyes and redox couple combinations. As the iodide electrolyte does not suffer from mass transport limitations in the photoanode films, the third semicircle is not seen in iodide-based DSCs for both the TiO<sub>2</sub>NN and P25 photoanodes. The

electron recombination lifetime,  $\tau_r$ , can be estimated from the Bode plots derived from EIS via the relationship of  $\tau_r = 1/2\pi f_{\max(\text{Bode})}$ , where  $f_{\max(\text{Bode})}$  is the maximum frequency in the intermediate-frequency region.<sup>24</sup> Analysis of the intermediate frequency semicircles, typically reflecting electron transfer processes occurring at the hetero-interface (Fig. 5a), reveals a lower frequency value for the TiO<sub>2</sub>NN-based cells than for P25-based cells for both cobalt and iodide electrolytes (Table 2). The estimated electron recombination times ( $\tau_r$ ) for the four cells are presented in Table 2. The  $\tau_r$  in the TiO<sub>2</sub>NN electrode is much larger than that in the P25 mesoporous electrode, which is in agreement with the higher PCE observed for the TiO<sub>2</sub>NN-based devices.<sup>53</sup> Hence, the recombination rate is significantly reduced when TiO<sub>2</sub>NN films are used.

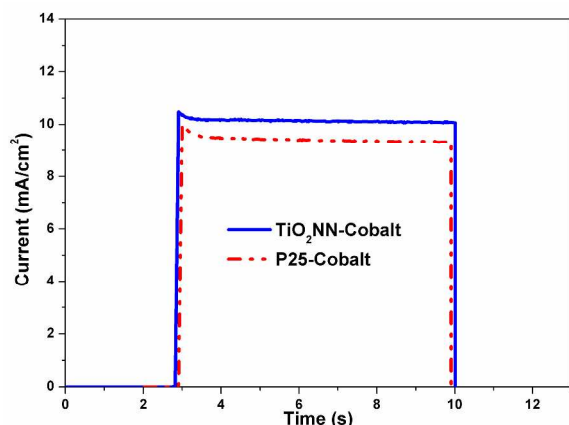


Fig. 4 Transient photocurrent measurement carried out under an illumination intensity of 100 mW/cm<sup>2</sup> for DSCs assembled with TiO<sub>2</sub>NN and P25 electrodes and the cobalt electrolyte (see footnotes to Table 1).

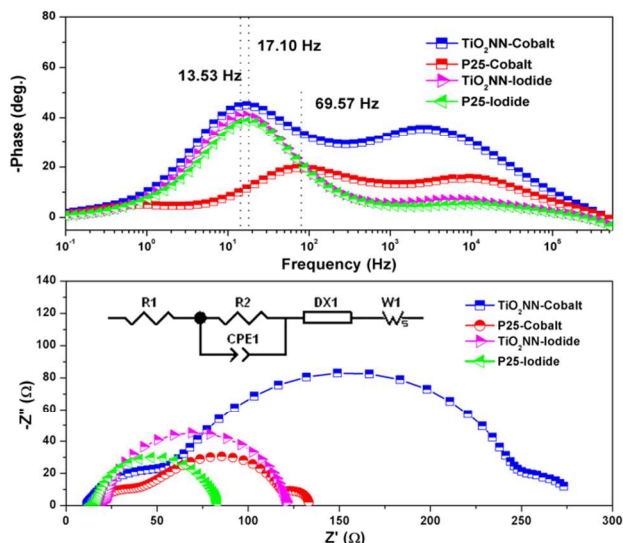


Fig. 5 EIS results presented as Bode (a) and Nyquist (b) plots for cells constructed with TiO<sub>2</sub>NN and P25 and either the cobalt or iodide-based electrolytes (see Table 1 footnotes) measured in the dark at -0.85 V bias.

The equivalent circuit model (TL-Open) shown in Fig. 5b was used to fit the Nyquist plot using the ZView software.<sup>54</sup>

The calculated diffusion resistance suggests that  $R_{\text{diff}}$  for TiO<sub>2</sub>NN-based cells is slightly lower than that of P25-based cells, indicating that the morphology of TiO<sub>2</sub>NN favours mass transport in photoanode films. For the cobalt electrolyte, the recombination resistance ( $R_{\text{cr}}$ ) of the TiO<sub>2</sub>NN-based cell (79 Ω) is 3.8 times larger than that for the P25-based cell (21 Ω), implying that electron recombination is much slower for the TiO<sub>2</sub>NN case. Similarly,  $R_{\text{cr}}$  of cell is larger for the iodide electrolyte when TiO<sub>2</sub>NN was used (87 Ω for TiO<sub>2</sub>NN and 53 Ω for P25). This result is in agreement with the dark current and Bode impedance analysis (see above). Calculation of the resistance to electron transport ( $R_t$ ) in the photoanode film (see Table 2), revealed that there is almost no difference of electron transport across TiO<sub>2</sub>NN and P25 film for both the iodide and cobalt electrolyte. The recombination resistance ( $R_{\text{cr}}$ ) at different bias voltage was also calculated by fitting Nyquist plot. Importantly, for the cobalt electrolyte the  $R_{\text{cr}}$  value is significantly higher over the bias voltage range from -0.65 to -0.90 V when TiO<sub>2</sub>NN is used as a photoanode instead of P25 (Fig. S1). Note also that although the  $R_{\text{cr}}$  value for the TiO<sub>2</sub>NN-based cell is slightly larger than that of P25-based cell for the iodide electrolyte, there is little or no difference in  $R_t$  for these two electrolytes (Fig. S2).

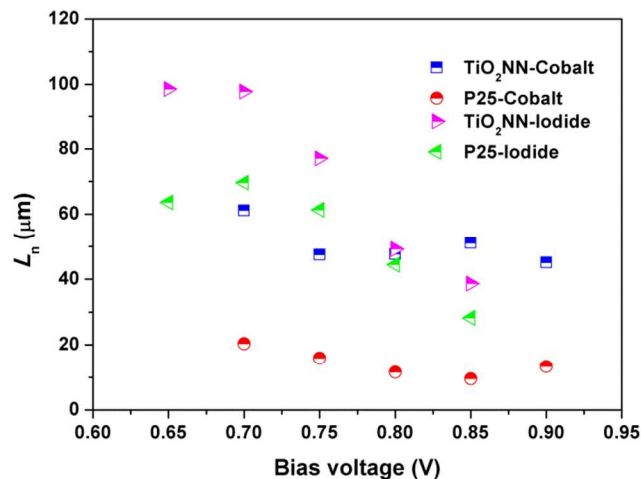
**Table 2** EIS parameters of four DSCs determined by fitting the experimental data according to the equivalent circuit model using the Zview software (shown in inset image of Fig. 5b).

Photo-anode	Dye/redox couple	$R_{\text{cr}}^a$ (Ω)	$R_t^b$ (Ω)	$R_{\text{diff}}$ (Ω)	$f_{\max(\text{Bode})}^d$ (Hz)	$\tau_r^e$ (ms)
TiO <sub>2</sub> NN MK2	[Co(bpy) <sub>3</sub> ] <sup>2+/3+</sup>	79	1.4	12	17	9.3
	N719 + I <sup>-</sup> /I <sub>3</sub> <sup>-</sup>	87	2.1	12	14	12
P25 MK2	[Co(bpy) <sub>3</sub> ] <sup>2+/3+</sup>	21	1.1	17	70	2.3
	N719 + I <sup>-</sup> /I <sub>3</sub> <sup>-</sup>	53	2.4	14	17	9.3

<sup>a</sup> $R_{\text{cr}}$  is denoted as the recombination resistance of DSCs. <sup>b</sup> $R_t$  means transport resistance. <sup>c</sup> $C_{\mu}$  represents chemical capacitance. <sup>d</sup> $f_{\max(\text{Bode})}$  is the maximum frequency in the intermediate-frequency region. <sup>e</sup> $\tau_r$  means electron recombination lifetime estimated from the Bode plots.

Taking into account recombination and charge transport together, the effective diffusion length ( $L_n$ ), defined as  $L_n = d\sqrt{R_{\text{cr}}/R_t}$ ,<sup>55</sup> was calculated at varying bias voltage ( $d$  represents the thickness of TiO<sub>2</sub>NN and P25 film). As shown in Fig. S1 and S2,  $R_{\text{cr}}$  and  $R_t$  increase with the decrease of bias voltage applied, in agreement with previous study.<sup>56</sup> Hence, the calculated  $L_n$  does not vary very drastically. For the cobalt electrolyte, the  $L_n$  values for the TiO<sub>2</sub>NN devices are approximately 3 times higher than for the P25 devices (Fig. 6). In contrast, TiO<sub>2</sub>NN devices have a slightly larger  $L_n$  values than P25 devices in iodide electrolyte (Fig. 6), but in keeping with the better performance of TiO<sub>2</sub>NN as photoanode in DSCs compared with P25. This result indicates that TiO<sub>2</sub>NN

significantly inhibits the interception of injected electrons by the  $[\text{Co}(\text{bpy})_3]^{3+}$  ions in the cobalt electrolyte.



**Fig. 6** Electron diffusion length ( $L_n$ ) as a function of  $V_{oc}$  for four solar cells fabricated using  $\text{TiO}_2\text{NN}$  and P25 films and either MK2 + cobalt or N719 + iodide electrolyte combinations. For the electrolyte compositions see footnotes to Table 1.

To examine the dynamics of electron recombination with reduced species in the electrolyte and electron transport across  $\text{TiO}_2\text{NN}$  film, IMPS/IMVS studies<sup>57</sup> were carried out under illumination using an LED light source ( $\lambda = 435$  nm) with light intensity ranging from 10 to 105  $\text{W}/\text{m}^2$ . The electron lifetimes ( $\tau_r$ ) and transport times ( $\tau_d$ ) for the  $\text{TiO}_2\text{NN}$  and P25-based DSCs in different electrolytes are plotted as functions of the open-circuit voltage and light intensities in Fig. 7. The IMVS curves show that the  $\text{TiO}_2\text{NN}$  films exhibit a significantly longer electron lifetime (slower recombination rate) than the mesoporous P25 films for the cobalt electrolyte whereas there is little difference for the iodide electrolyte. Combining this result with the chemical capacitance measurement (Fig. S1), we can conclude that for the thinner 3  $\mu\text{m}$  films recombination for the quasi-1D  $\text{TiO}_2\text{NN}$  photoanodes is significantly reduced compared with the P25-based photoanodes. This is in agreement with EIS results. However, for the iodide-based devices, where thicker  $\text{TiO}_2\text{NN}$  and P25 photoanodes (6  $\mu\text{m}$ ) were used, no difference in the rates of electron recombination was observed. In addition, the electron transport time and electron diffusion coefficient ( $D_n = d^2/4\tau_d$ ),<sup>58</sup>  $d$  and  $\tau_d$  denotes thickness of film and electron transport time derived from IMPS measurement) across  $\text{TiO}_2\text{NN}$  film were determined. According to Fig. 7b and Fig. S4, the  $\text{TiO}_2\text{NN}$  film shows the same transport time with P25 in these two sensitized systems, again in agreement with the EIS analysis.

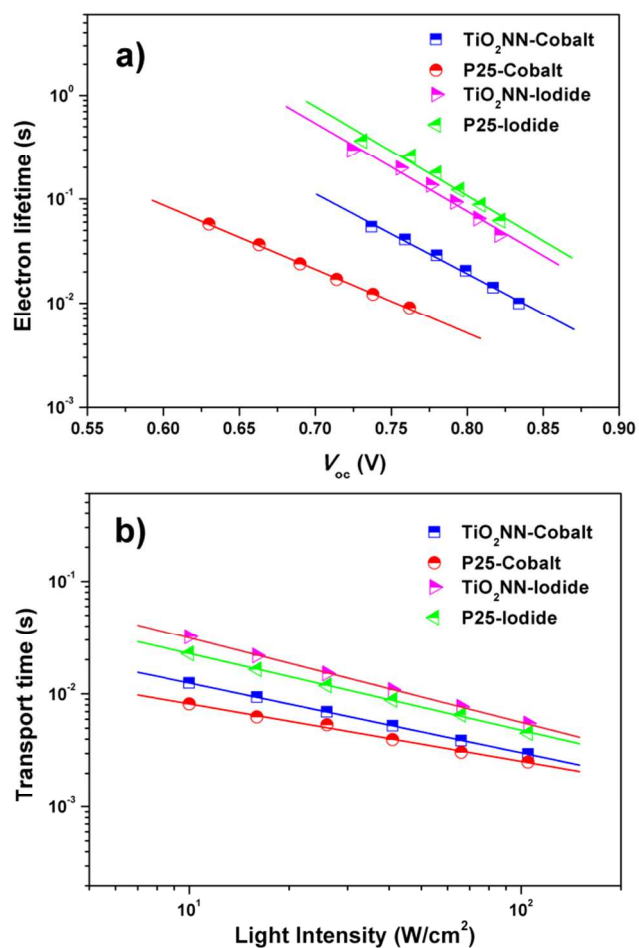


**Fig. 7** Incident light intensity dependence of the recombination time constant (a) and transport time constant (b) for solar cells based on  $\text{TiO}_2\text{NN}$  and P25 at 435 nm LED illumination.

## Conclusion

In summary, a quasi-one-dimensional  $\text{TiO}_2$  nanobundle network has been developed for application as a hierarchical nanostructure assembly in dye sensitized solar cells. For the MK2 dye and cobalt redox mediator-based electrolyte, the efficiency achieved (7.7%) was higher than that of P25 (only 6.3%). Detailed analysis of the films and devices through IPCE, EIS and IMVS measurements led to the conclusion that the excellent performance of the  $\text{TiO}_2\text{NN}$ -cobalt electrolyte based devices can be attributed their increased scattering ability, the suppression of interfacial electron recombination and effective mass transport of the redox couples through the films. For the iodide electrolytes, the  $\text{TiO}_2$  network-based DSCs were found to show comparable to photovoltaic performance to corresponding DSCs based on P25. Our results suggest that the quasi-one-dimensional nanobundle network is a promising DSC photoanode material owing to its special morphological structure. The development of highly ordered quasi-one-dimensional nanobundle network is under investigation.

## Acknowledgements

We acknowledge financial support from the Australian Solar Institute, the Victorian State Government Department of Primary Industry, Bluescope Steel, Innovia Films, Innovia Security and Bosch (Victorian Organic Solar Cells consortium). Support of the Australian Centre for Advanced Photovoltaics by the Australian Government through the Australian Renewable Energy Agency (ARENA) is also gratefully acknowledged. Xin Li acknowledges financial support from Specialized Research Fund for the Doctoral Program of Higher Education (20122302110043) and Cunku Dong from the Joint Educational PhD Program of Chinese Scholarship Council (CSC). We are grateful to the Monash Centre for Electron Microscopy for the use of the SEM facilities.

## Notes and references

<sup>a</sup>School of Chemistry, Monash University, Victoria 3800, Australia. E-mail: leone.spiccia@monash.edu

<sup>b</sup>Department of Chemistry, Harbin Institute of Technology, Harbin 150001, China. E-mail: lixin@hit.edu.cn

<sup>c</sup>Department of Materials Engineering, Monash University, Victoria 3800, Australia.

<sup>d</sup>Commonwealth Scientific and Industrial Research Organization, Materials Science and Engineering, Flexible Electronics Theme, Clayton South, Victoria 3169, Australia

<sup>e</sup>Melbourne Centre for Nanofabrication, 151 Wellington Road, Clayton, VIC 3168, Australia

†Electronic Supplementary Information (ESI) available: [details of any supplementary information available should be included here]. See DOI: 10.1039/b000000x/

- B. O'Regan and M. Grätzel, *Nature*, 1991, **353**, 737.
- M. Grätzel, *Nature*, 2001, **414**, 338.
- A. Yella, H. W. Lee, H. N. Tsao, C. Yi, A. K. Chandiran, M. K. Nazeeruddin, E. W. G. Diau, C. Y. Yeh, S. M. Zakeeruddin and M. Grätzel, *Science*, 2011, **334**, 629.
- T. Daeneke, T.-H. Kwon, A. B. Holmes, N. W. Duffy, U. Bach and L. Spiccia, *Nature Chem.*, 2011, **3**, 211.
- T. Daeneke, A. J. Mozer, Y. Uemura, M. Fekete, N. Koumura, U. Bach and L. Spiccia, *J. Am. Chem. Soc.*, 2012, **134**, 16925.
- T. Daeneke, A. Mozer, T.-H. Kwon, N. Duffy, A. B. Holmes, U. Bach, L. Spiccia, *Energy Environ. Sci.*, 2012, **5**, 7090.
- M. K. Kashif, J. C. Axelson, N. Duffy, C. M. Forsyth, C. J., Chang, J. R. Long, L. Spiccia and U. Bach, *J. Am. Chem. Soc.*, 2012, **134**, 16646.
- M. K. Kashif, M. Nippe, C. M. Forsyth, C. J. Chang, J. R. Long, L. Spiccia and U. Bach, *Angew Chem. Int. Ed.*, 2013, **52**, 5527.
- T. Daeneke, Y. Uemura, N. Duffy, A. Mozer, N. Koumura, U. Bach and L. Spiccia, *Adv. Mater.*, 2012, **24**, 1222.
- W. Xiang, F. Huang, Y.-B. Cheng, U. Bach and L. Spiccia, *Energy Environ. Sci.*, 2013, **6**, 121.
- A. Hagfeld, G. Boschloo, L. Sun, L. Kloo, H. Pettersson, *Chem. Rev.*, 2010, **110**, 6595.
- Q. L. Huang, G. Zhou, L. Fang, L. P. Hu and Z. S. Wang, *Energy Environ. Sci.*, 2011, **4**, 2145.
- M. Law, L. E. Greene, J. C. Johnson, R. Saykally and P. Yang, *Nat. Mater.*, 2005, **4**, 455.
- B. Liu and E. S. Aydil, *J. Am. Chem. Soc.*, 2009, **131**, 3985.
- A. B. F. Martinson, J. W. Elam, J. T. Hupp and M. J. Pellin, *Nano Lett.*, 2007, **7**, 2183.
- G. K. Mor, K. Shankar, M. Paulose, O. K. Varghese and C. A. Grimes, *Nano Lett.*, 2006, **6**, 215.
- L. L. Li, Y. J. Chen, H. P. Wu, N. S. Wang and E. W. G. Diau, *Energy Environ. Sci.*, 2011, **4**, 3420.
- G. Melcarne, L. De Marco, E. Carlino, F. Martina, M. Manca, R. Cingolani, G. Gigli and G. Ciccarella, *J. Mater. Chem.*, 2010, **20**, 7248.
- P. Sun, X. Zhang, X. Liu, L. Wang, C. Wang, J. Yang and Y. Liu, *J. Mater. Chem.*, 2012, **22**, 6389.
- X. Feng, K. Zhu, A. J. Frank, C. A. Grimes and T. E. Mallouk, *Angew. Chem. Int. Ed.*, 2012, **51**, 2727.
- A. Kumar, A. R. Madaria and C. Zhou, *J. Phys. Chem. C*, 2010, **114**, 7787.
- Q. F. Zhang and G. Z. Cao, *Nano Today*, 2011, **6**, 91.
- A. I. Hochbaum and P. Yang, *Chem. Rev.*, 2010, **110**, 527.
- X. Wang, Y. Liu, X. Zhou, B. Li, H. Wang, W. Zhao, Hong Huang, C. Liang, X. Yu, Z. Liu and H. Shen, *J. Mater. Chem.*, 2012, **22**, 17531.
- Z. Zhou, J. Fan, X. Wang, W. Zhou, Z. Du, S. Wu, *ACS Appl. Mater. Interfaces*, 2011, **3**, 4349.
- M. McCune, W. Z., Y. Deng, *Nano Lett.*, 2012, **12**, 3656.
- J.-Y. Liao, B.-X. Lei, H.-Y. Chen, D. B. Kuang, C.-Y. Su, *Energy Environ. Sci.*, 2012, **5**, 5750.
- H. Zhang, X. Liu, Y. Li, Q. Sun, Y. Wang, B. J. Wood, P. Liu, D. Yang, H. Zhao, *J. Mater. Chem.*, 2012, **22**, 2465.
- C.-T. Wu, J.-J. Wu, *J. Mater. Chem.*, 2011, **21**, 13605.
- P. S. Archana, E. Naveen Kumar, C. Vijila, S. Ramakrishna, M. M. Yusoff and R. Jose, *Dalton Trans.*, 2013, **42**, 1024.
- Zhu, A. S. Nair, S. Yang, S. Peng and S. Ramakrishna, *J. Mater. Chem.*, 2011, **21**, 12210.
- L. Yang and W. W.-F. Leung, *Adv. Mater.*, 2011, **23**, 4559.
- K. Fujihara, A. Kumar, R. Jose, S. Ramakrishna and S. Uchida, *Nanotechnology*, 2007, **18**, 365709.
- C.-H. Ku and J.-J. Wu, *Appl. Phys. Lett.*, 2007, **91**, 093117
- X. Y. Gan, X. M. Li, X. D. Gao, F. W. Zhuge and W. D. Yu, *Thin Solid Films*, 2010, **518**, 4809.
- X. A. Pan, C. H. Chen, K. Zhu and Z. Y. Fan, *Nanotechnology*, 2011, **22**, 235402.
- V. S. Saji and M. Pyo, *Thin Solid Films*, 2010, **518**, 6542.
- P. Joshi, L. Zhang, D. Davoux, Z. Zhu, D. Galipeau, H. Fong and Q. Qiao, *Energy Environ. Sci.*, 2010, **3**, 1507.
- X. Wang, S. Karanjit, L. Zhang, H. Fong, Q. Qiao and Z. Zhu, *Appl. Phys. Lett.*, 2011, **98**, 082114.
- P. S. Archana, R. Jose, C. Vijila and S. Ramakrishna, *J. Phys. Chem. C*, 2009, **113**, 21538.
- Y. Bai, H. Yu, Z. Li, R. Amal, G. Qi. Lu and L. Wang, *Adv. Mater.*, 2012, **24**, 5850.
- W.-Q. Wu, J.-Y. Liao, H.-Y. Chen, X.-Y. Yu, C.-Y. Su and D.-B. Kuang, *J. Mater. Chem.*, 2012, **22**, 18057.
- H. B. Wu, H. H. H. and X. W. Lou, *Adv. Mater.* 2012, **24**, 2567.

44. M. K. Nazeeruddin, P. Péchy, T. Renouard, S. M. Zakeeruddin, R. Humphry-Baker, P. Comte, P. Liska, L. Cevey, E. Costa, V. Shklover, L. Spiccia, G. B. Deacon, C. A. Bignozzi, M. Grätzel, *J. Am. Chem. Soc.*, 2001, **123**, 1613.
45. W. Xiang, A. Gupta, M. K. Kashif, N. Duffy, A. Bilic, R. A. Evans, L. Spiccia, U. Bach, *ChemSusChem*, 2013, **6**, 256.
46. Y. Sun, A. C. Onicha, M. M. F. N. Castellano, *ACS Appl. Mater. Interfaces*, 2010, **2**, 2039.
47. A. Zaban, A. Meier, B. A. Gregg, *J. Phys. Chem. B* 1997, **101**, 7985.
48. M. Du, X.-J. Zhao, H. Cai, Z. Kristallogr. NCS, 2004, **219**, 463.
49. J. J. Nelson, T. J. Amick and C. M. Elliott, *J. Phys. Chem. C*, 2008, **112**, 18255.
50. J. van de Lagemaat, N. G. Park and A. J. Frank, *J. Phys. Chem. B*, 2000, **104**, 2044.
51. Q. Wang, J. E. Moser and M. Gratzel, *J. Phys. Chem. B*, 2005, **109**, 14945.
52. R. Kern, R. Sastrawan, J. Ferber, R. Stangl and J. Luther, *Electrochim. Acta*, 2002, **47**, 4213.
53. J.-F. Qian, P. Liu, Y. Xiao, Y. Jiang, Y.-L. Cao, X.-P. Ai and H.-X. Yang, *Adv. Mater.*, 2009, **21**, 3663.
54. a) M. C. Lefebvre, R. B. Martin and P. G. Pickup, *Electrochem. Solid-State Lett.*, 1999, **2**, 259; b) R. Makharia, M. F. Mathias and D. R. Baker, *J. Electrochem. Soc.*, 2005, **152**, A970.
55. M. J. Carnie, C. Charbonneau, P. R. F. Barnes, M.L. Davies, I. Mabbett, T. M. Watson, B. C. O'Regan and D. A. Worsley, *J. Mater. Chem. A*, 2013, **1**, 2225.
56. M. J. Carnie, C. Charbonneau, P. R. F. Barnes, M. L. Davies, I. Mabbett, T. M. Watson, B. C. O'Regan and D. A. Worsley, *J. Mater. Chem. A*, 2013, **1**, 2225.
57. G. Schlichthorl, S. Y. Huang, J. Sprague and A. J. Frank, *J. Phys. Chem. B*, 1997, **101**, 8141.
58. C. He, L. Zhao, Z. Zheng and F. Lu, *J. Phys. Chem. C*, 2008, **112**, 18730.

## Table of Contents Entry:

A titania-nanobundle-network minimizes electron recombination in DSCs, allows fast diffusion of the  $[\text{Co}(\text{bpy})_3]^{2+/3+}$  couple through the photoanode and results in a 7.7% efficiency.

